

Combining multispectral polarized light imaging and confocal microscopy for localization of nonmelanoma skin cancer

Anna N. Yaroslavsky

Harvard Medical School
Massachusetts General Hospital
Wellman Laboratories of Photomedicine
Department of Dermatology
Boston, Massachusetts 02114
E-mail: yaroslav.helix.mgh.harvard.edu

Jose Barbosa

Harvard Medical School
Massachusetts General Hospital
Wellman Laboratories of Photomedicine
Boston, Massachusetts 02114
and
Northeastern University
Department of Electrical and Computer Engineering
Boston, Massachusetts

Victor Neel

Harvard Medical School
Massachusetts General Hospital
Wellman Laboratories of Photomedicine
Boston, Massachusetts 02114

Charles DiMarzio

Northeastern University
Department of Electrical and Computer Engineering
Boston, Massachusetts

R. Rox Anderson

Harvard Medical School
Massachusetts General Hospital
Wellman Laboratories of Photomedicine
Boston, Massachusetts 02114

1 Introduction

Advances in the development of optical imaging modalities¹⁻³ have facilitated efforts to employ these techniques for noninvasive detection and treatment guidance of different pathological conditions. In general, the turbidity of tissue creates major challenges for optical *in vivo* spectroscopy and imaging. However, reflectance imaging techniques, like multispectral polarized light macroimaging and confocal microscopy (CM), are well suited for skin cancer detection and demarcation. Confocal reflectance microscopy was introduced to the field of dermatology in the 1990s.⁴ Since then it has been used to study different skin disorders.^{5,6} Confocal microscopy is a technique where the specimen is pointwise illuminated by a focused beam of light. An image is recorded by scanning the beam focus through a plane in the specimen, and the reflected light from the specimen is focused onto a small detector aperture. The light source, illuminated spot, and detector aperture are placed in optically conjugated focal planes. Optical

Abstract. Multispectral polarized light imaging (MSPLI) enables rapid inspection of a superficial tissue layer over large surfaces, but does not provide information on cellular microstructure. Confocal microscopy (CM) allows imaging within turbid media with resolution comparable to that of histology, but suffers from a small field of view. In practice, pathologists use microscopes at low and high power to view tumor margins and cell features, respectively. Therefore, we study the combination of CM and MSPLI for demarcation of nonmelanoma skin cancers. Freshly excised thick skin samples with nonmelanoma cancers are rapidly stained with either toluidine or methylene blue dyes, rinsed in acetic acid, and imaged using MSPLI and CM. MSPLI is performed at 630, 660, and 750 nm. The same specimens are imaged by reflectance CM at 630, 660, and 830 nm. Results indicate that CM and MSPLI images are in good correlation with histopathology. Cytological features are identified by CM, and tumor margins are delineated by MSPLI. A combination of MSPLI and CM appears to be complementary. This combined *in situ* technique has potential to guide cancer surgery more rapidly and at lower cost than conventional histopathology. © 2005 Society of Photo-Optical Instrumentation Engineers. [DOI: 10.1117/1.1854173]

Keywords: multispectral imaging; confocal microscopy; skin cancer; dyes.

Paper 04108 received Jun. 23, 2004; revised manuscript received Aug. 5, 2004; accepted for publication Aug. 11, 2004.

sectioning occurs as out-of-focal-plane back-scattered light is rejected by a pinhole placed in front of a detector. Optical sectioning makes it possible to record images of thin layers within tissue. Confocal microscopy allows imaging within turbid media with high resolution (lateral $\sim 1 \mu\text{m}$, axial (section thickness) ~ 3 to $5 \mu\text{m}$), which is comparable to histology. The major disadvantage of confocal microscopy as a detection and guidance tool for cancer surgery is its small field of view (typically up to about 0.3 mm). By sacrificing axial resolution up to $\sim 30 \mu\text{m}$, it is possible to enlarge the field of view up to 2 mm. But even a 2-mm field of view is much smaller than the size of most lesions. To examine the entire suspected cancerous area using CM, a sequence of images must be captured and stitched together. This process takes time and motion artifacts may distort the resulting image.

Multispectral polarized light imaging (MSPLI)⁷ is a simple and inexpensive technique for skin tumor imaging. The technique provides the means to differentiate effectively between endogenous (blood, melanin, etc.) and exogenous (dye) chro-

Address all correspondence to Anna N. Yaroslavsky, Dermatology, Wellman Labs for Photomedicine, MGH BHX 630, 55 Fruit Street, Boston, MA 02114. Tel: 617 726 1590; Fax: 617 724 2075; E-mail: yaroslav@helix.mgh.harvard.edu

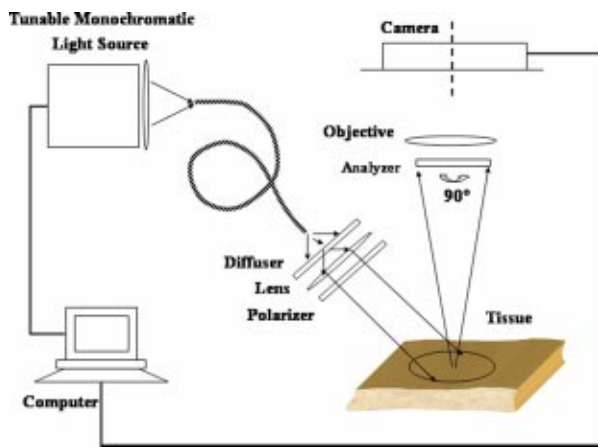


Fig. 1 Schematic diagram of multispectral polarized light imaging system.

mophores absorbing in different spectral domains and is capable of obtaining superficial images ($\sim 150 \mu\text{m}$ in the visible spectral range) of thick tissue layers. It is relatively insensitive to small shifts in the position of the imaged object. A combination of the large field of view and sufficient lateral resolution enables rapid examination of large surfaces, thus facilitating tumor margin delineation. However, morphology of individual cells and fine structures cannot be resolved using MSPLI. Thus, the multispectral polarized light imaging approach naturally lends itself to a combination with the confocal reflectance microscopy technique, which can be used by a pathologist in cases when high-resolution images of small suspicious areas are required. Such combination may become a powerful tool for cancer detection and demarcation.

In this study, the possibility of combining multispectral polarized light macroimaging and confocal microscopy for delineating nonmelanoma skin cancers, i.e., basal cell carcinoma (BCC) and squamous cell carcinoma (SCC), was investigated. 23 freshly excised thick skin samples with nonmelanoma skin cancers were stained with either toluidine blue O (TB) or methylene blue (MB), rinsed in acetic acid (AA), and imaged using CM and MSPLI systems. The acquired images were processed and compared to each other and to histopathology. The ability of this combined technique to delineate tumor margins and distinguish different tissue structures was evaluated.

2 Materials and Methods

2.1 Multispectral Polarized Light Imaging

A schematic of the multispectral polarized light imaging system is presented in Fig. 1. We used a xenon arc lamp (Lambda LS, Sutter Incorporated, Novato, California) combined with interference filters as a narrowband light source and a charge-coupled device (CCD) camera (CoolSNAP Monochrome Photometrics, Roper Scientific Incorporated, Tuscon, Arizona) as an imaging device. Linearly polarizing filters were introduced into the pathways of incident light and light collected by the camera to enable imaging using co- and cross-polarized scattered light. The automated system provided rapid image acquisition and processing at multiple wavelengths, large field

of view (maximum $2.9 \times 2.7 \text{ cm}$), and lateral resolution of approximately $30 \mu\text{m}$. The incident power density did not exceed $150 \mu\text{W}/\text{cm}^2$.

To image a superficial tissue layer of approximately 150 to $200 \mu\text{m}$,^{7,8} two images were acquired using the remitted light polarized in the directions parallel (I_{\parallel}) and perpendicular (I_{\perp}) to the polarization of incident light.^{7,8} It has been shown previously that the difference image ($I_{\delta} = I_{\parallel} - I_{\perp}$) is produced mainly by single scattered light.⁷⁻⁹ The images were acquired from the dermal side of the specimens at wavelengths of the phenothiazine dyes absorption, 630 and 660 nm, and at the reference wavelength of 750 nm. The acquired images were processed in the following way. The difference images I_{δ} were calculated for each wavelength. To reject the background signal, the resulting superficial macroimages, $I_{\Delta}^{\lambda} = I_{\delta}^{\lambda} - I_{\delta}^{\lambda_r}$ for $\lambda = 630, 660 \text{ nm}$; $\lambda_r = 750 \text{ nm}$, were computed, analyzed, and compared to CM images and histopathology.

2.2 Confocal Microscopy

A schematic of the confocal imaging system is presented in Fig. 2. For the experiments, a commercial reflectance CM (Vivascope 2000, Lucid Incorporated, Henrietta, New York) was modified in the following way. In addition to the existing infrared laser diode ($\lambda = 830 \text{ nm}$), the light from an argon-ion laser (Innova 100, Coherent, California) pumped dye laser (Coherent 599, Coherent, California) was coupled into the microscope. To optimize broadband visible and infrared light transmission through the system, several optical components of the original configuration, i.e., polarizing beamsplitter, lenses, and quarter waveplate, were replaced by high-performance substitutes. Integration of an additional light source allowed imaging in the wavelength range from 600 to 830 nm and enabled localization of MB and TB in thick skin excisions with nonmelanoma cancers. Confocal images were acquired at wavelengths of 630, 660, and 830 nm. Water immersion $20 \times / 0.75$ objective (Nikon, Japan) was used in all experiments. The system provided an axial resolution of 5 to $6 \mu\text{m}$, and lateral resolution of 1.2 to $1.5 \mu\text{m}$ in the range from 620 to 830 nm. The incident power for each wavelength was adjusted not to exceed 12 mW. Confocal images were acquired from the dermal side of the samples at depths of 10 to $40 \mu\text{m}$ beneath the surface of the tissue. The depth of confocal imaging was chosen based on location, size, and surface curvature of the investigated part of the specimen. Single confocal images covered the area of $800 \times 600 \mu\text{m}$. To compare the results with macroscopic polarized light images, confocal mosaics were created from single confocal images. These mosaics covered an area of $8 \times 6 \text{ mm}$. The resulting confocal images and mosaics were compared to MSPLI and histopathology.

2.3 Tissue Preparation

Fresh thick skin specimens containing nonmelanoma cancer were obtained from Mohs micrographic surgeries. In total, 23 samples were used for the experiments. The study was performed according to a protocol approved by the institutional review board of Massachusetts General Hospital. Discarded tumor material that remained after Mohs histological analysis was used. The tissue was frozen in the microcryotome and thawed immediately before the experiment. Several contrast

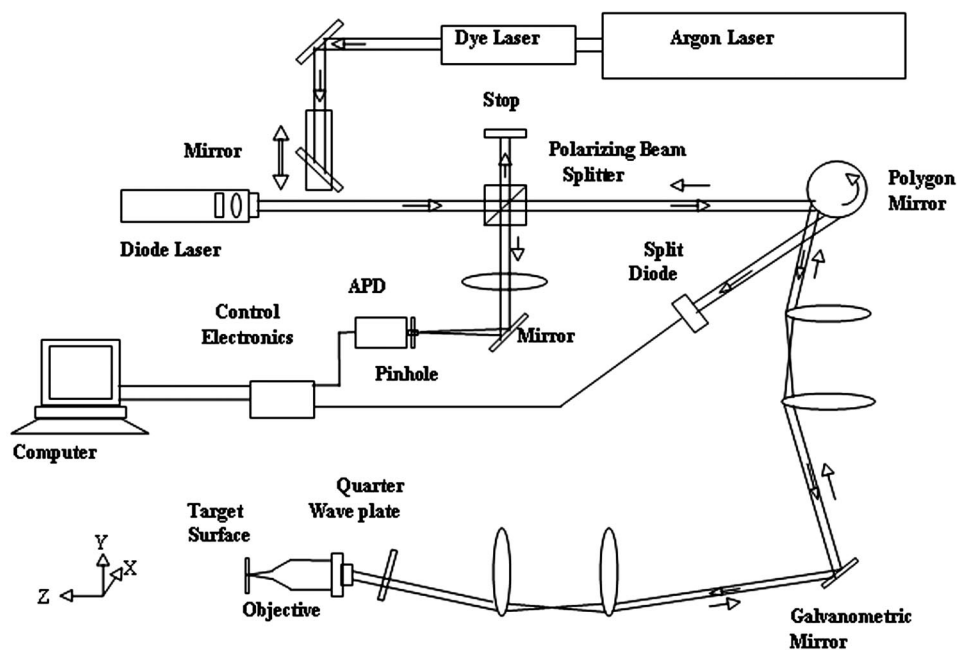


Fig. 2 Schematic diagram of the confocal microscope.

agents, including methylene blue, toluidine blue O, and acetic acid, were applied to the tissue to enhance the contrast of a lesion with respect to the healthy tissue. MB and TB are preferentially retained in carcinoma cells.¹⁰ These dyes have similar chemical structures and physicochemical properties. Absorption band in the 550- to 700-nm region determines the blue color of MB and TB. Acetic acid is often applied for confocal examination of different cancer types.^{6,11} Washing with acetic acid leads to chromatin compaction inside the cell nuclei. Compacted chromatin increases light scattering by the nuclei, thus enhancing the contrast of the image. For the experiments, each specimen was submerged for 10 to 20 min in isotonic Dulbecco's phosphate-buffered solution (DPBS) of MB or TB and for 2 min in 5% AA. 13 samples were stained using MB and AA (11 BCC and 2 SCC) and 10 samples using TB and AA (7 BCC and 3 SCC). After the excessive dye was rinsed off the samples, the intact tissue was imaged using CM and MSPLI systems. For imaging, cancer specimens were placed on a glass slide and covered with a cover slip. A drop of saline solution was added to prevent drying of the sample. To enable comparison of the results to histopathology, the images were acquired from the dermal side of the specimens.

2.4 Comparison of the Images to Histopathology

The resulting MSPLI and CM images were qualitatively compared to each other and to the last histological frozen section processed during Mohs surgery. Preparation of histological horizontal sections is described in detail elsewhere.^{12,13} Ideally, the last frozen section generated during surgery should reproduce the features of the reflectance polarization image acquired from the remaining discarded piece of tissue that we use for the experiments (see Fig. 3). However, the thickness of an optical section is approximately 150 to 200 μm . It is 30 to 40 times thicker than the histological section, which is only 5 μm thick. This difference in thickness may contribute to the

quantitative discrepancies in the size of the tumors determined from the MSPLI and histopathology. Confocal images were acquired from depths of 10 to 40 μm below the surface of the tissue. Therefore, they should closely resemble the last histological frozen section processed during Mohs surgery. However, the ideal correlation cannot be expected, as the spatial gap of 10 to 40 μm between the frozen and confocal sections is on the order of one to several cell dimensions. For these reasons, quantitative comparison of the images to histopathology could not be done in a straightforward manner and was not attempted in this work. However, due to the obvious similarities of the tissue features present in histological slides, CM, and MSPLI images, visual qualitative comparison of the tumor shape, size, and margins was performed.

3 Results and Discussion

Nodular basal cell carcinoma is the most frequently occurring type of nonmelanoma skin cancers. Confocal and polarized

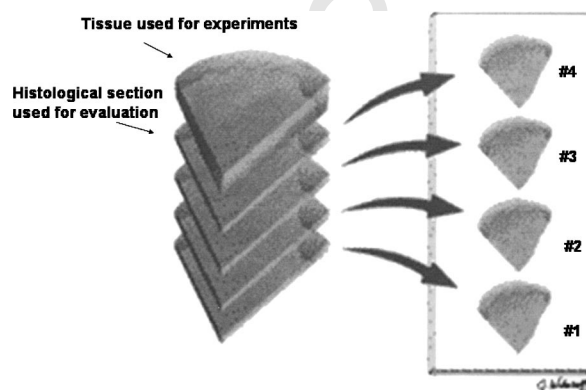


Fig. 3 Preparation of the horizontal histological frozen sections.

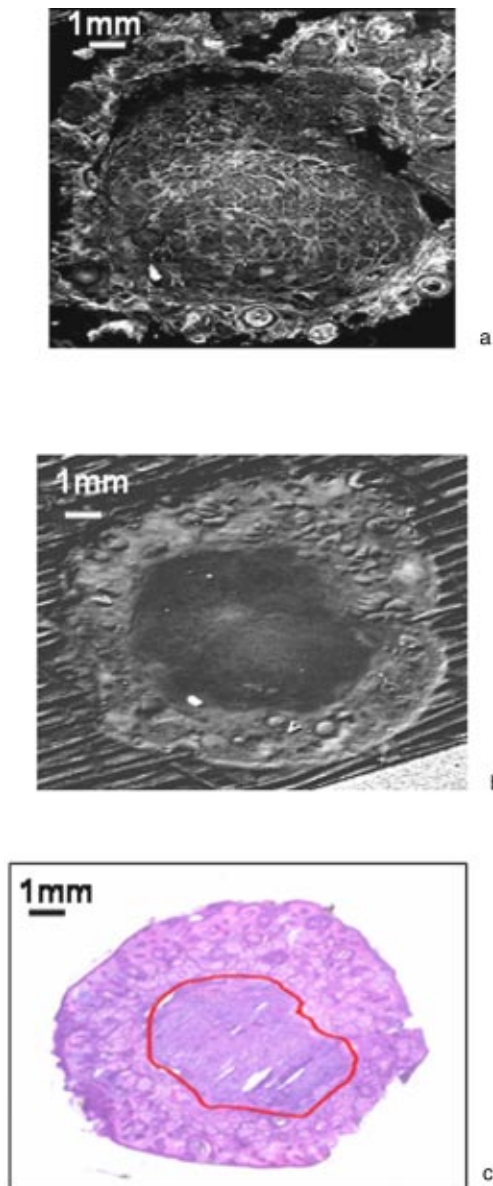


Fig. 4 Images of nodular BCC stained in 0.2 mg/ml aqueous solution of MB: (a) confocal mosaic acquired at 660 nm; (b) superficial macroimage acquired at 660 nm; and (c) histological frozen section. Tumor margins in (c) as determined by a Mohs surgeon are outlined with red line (color online only).

light superficial images of a representative specimen with nodular basal cell carcinoma stained in 0.2 mg/ml aqueous solution of MB acquired at 660 nm are presented in Figs. 4(a) and 4(b), respectively. Contrast of the tumor with respect to normal tissue was sufficient for reliable delineation of the cancer margins in both CM and MSPLI images. CM and MSPLI images, presented in Figs. 4(a) and 4(b), correlate well with corresponding histopathology, presented in Fig. 4(c). Comparison of the images in Figs. 4(a) and 4(b) shows that a CM mosaic provides more information than MSPLI on the arrangement and structure of separate tumor lobules, but is not capable of visualizing the complete sample, whereas an MSPLI image provides a larger field of view, but does not

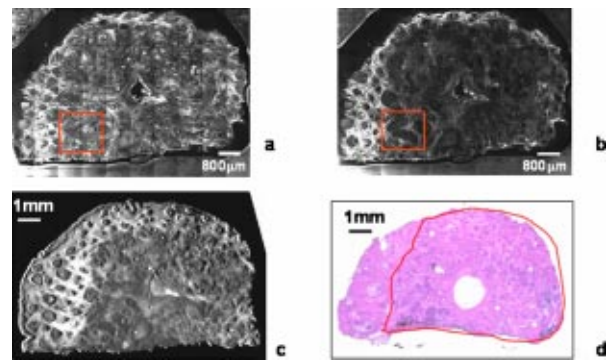


Fig. 5 Images of infiltrative BCC stained in 0.2 mg/ml aqueous solution of TB. (a) Confocal mosaic acquired at 830 nm. (b) Confocal mosaic acquired at 630 nm. (c) Superficial macroimage acquired at 630 nm. Red square in the confocal mosaics outlines the area presented in the confocal images in Figs. 6(a) and 6(b). (d) Histological frozen section. Tumor margins in (d) as determined by Mohs surgeon are outlined with red line (color online only).

show single tumor nests. The differences in resolution can be explained mainly by a difference in the optical section thickness between CM and MSPLI. The optical section thickness of each confocal image is ~ 5 to $6 \mu\text{m}$, approximately 30 to 40 times less than that of each MSPLI macroimage. Skin tumor excisions are thicker in the center and thinner at the edges. Therefore, it is usually not feasible to create a CM mosaic over the whole sample including the boundaries, whereas in the superficial macroimage, the complete sample is visualized. Another practical factor limiting confocal imaging is that CM requires the imaged sample surface to be held flat, which is difficult to achieve for a large surgical tissue sample. In contrast, MSPLI imaging does not require the sample surface to be flattened.

Infiltrative BCC tumors are a common variant of BCC that typically have thin strands or cords of tumor cells extending into the surrounding dermis. This type of tumor is usually hard to delineate. A surgical excision specimen with an infiltrative BCC was stained using aqueous solution of TB (0.2 mg/ml) and imaged at the wavelength of 630 nm, which is within the absorption band of the dye, and at 830 nm, where absorption of the dye is negligible. Confocal mosaics of the acquired images are presented in Figs. 5(a) and 5(b). It is difficult to localize the dye in Fig. 5(a) (confocal mosaic at 830 nm), while the dark areas in Fig. 5(b) (confocal mosaic at 630 nm) clearly demarcate areas of high dye concentration, corresponding to tumor. As in the case shown in Fig. 4 of a nodular BCC stained in MB, the confocal mosaic at 630 nm and the superficial polarized light image acquired at the same wavelength [Fig. 5(c)] are remarkably similar. Comparison of these two images with the last frozen section processed during Mohs surgery, presented in Fig. 5(d), demonstrates good correlation with histopathology. However, due to inherently lower resolution, the separate tumor lobules that are clearly visible in the CM mosaic can hardly be seen in the superficial macroimage. This case illustrates the value of combining CM and MSPLI to see both the small tumor lobules and the wider field tumor borders, respectively.

Confocal images presented in Figs. 6(a) and 6(b) are taken from the squares outlined in the CM mosaics at 830 and 630

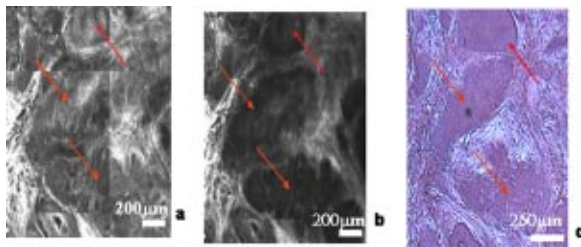


Fig. 6 Images of infiltrative BCC stained in 0.2 mg/ml aqueous solution of MB. Red arrows point to the locations of the tumor lobules. (a) Confocal image at 830 nm taken from the red square area of the mosaic presented in Fig. 3(a). (b) Confocal image at 660 nm taken from the red square area of mosaic presented in Fig. 3(b). (c) Histological frozen section (color online only).

nm, shown in Figs. 5(a) and 5(b). Corresponding histopathology is shown in Fig. 6(c). These confocal images were acquired at the margin of the tumor and contained several tumor lobules (red arrows) mixed with areas of healthy tissue. Margins of the tumor can hardly be delineated in the image acquired at 830 nm, whereas in the image acquired at 630 nm, the tumor is much darker than healthy tissue and can be easily demarcated. Comparison of the image at 630 nm [Fig. 6(b)] to frozen H and E section [Fig. 6(c)] confirms that position and shape of single tumor lobules is determined correctly by confocal microscopy.

In Fig. 7, images of invasive squamous cell carcinoma, stained using 0.1 mg/ml aqueous solution of TB, are presented. A polarized macroimage acquired at 630 nm and corresponding histological section are shown in Figs. 7(a) and 7(b). The shape and the size of the tumor that appears dark in the macroimage correspond well to that outlined with red marker in the histology. A confocal image of part of the cancerous area acquired at 630 nm and corresponding histopathology are presented in Figs. 7(c) and 7(d), respectively. Morphological appearance of the tumor microstructure is very

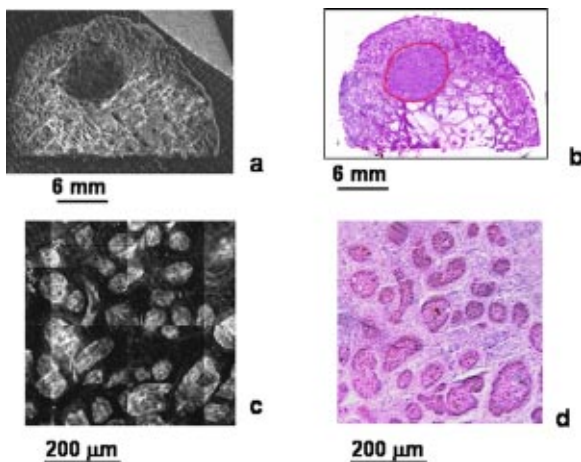


Fig. 7 Images of invasive SCC stained in 0.1 mg/ml aqueous solution of TB. (a) Superficial macroimage acquired at 630 nm. (b) Histological frozen section. Tumor margins in (b) as determined by a Mohs surgeon are outlined with red line. (c) Confocal image of cancer acquired at 630 nm. (d) Magnified image of the histological frozen section taken from the same area as presented in Fig. 7(c) (color online only).

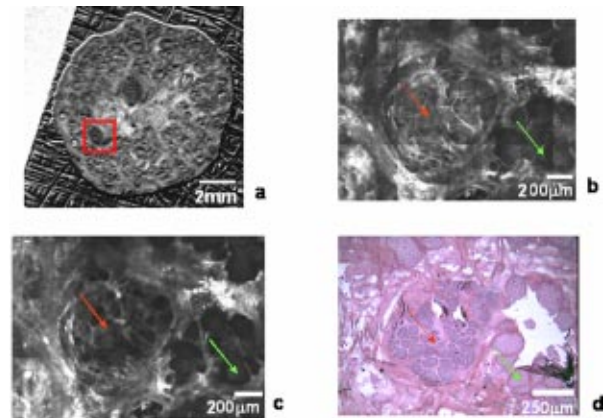


Fig. 8 Images of micronodular BCC stained in 0.2 mg/ml aqueous solution of MB. (a) Superficial macroimage acquired at 660 nm. Red square outlines the area presented in confocal images and histopathology in Figs. 8(b), 8(c), and 8(d). (b) Confocal image at 830 nm taken from the red square area of the macroimage presented in Fig. 8(a). (c) Confocal image at 660 nm taken from the red square area of the macroimage presented in Fig. 8(a). (d) Histological frozen section. Red arrow shows the location of tumor lobules; green arrow shows sebaceous glands (color online only).

similar in the confocal image and histology. Tumor cells appear bright due to scattering enhanced by acetic acid. Location and shape of the tumor lobules correlates well with those in the H and E stained frozen section. This example shows that a combination of topical staining using phenothiazine dyes and rinsing in AA may further enhance the similarities in the appearance of the acquired images and histopathology, thus simplifying interpretation of macro- and confocal images.

In Fig. 8(a) a polarized light macroimage of a basal cell carcinoma specimen stained in 0.2 mg/ml aqueous solution of MB acquired at 660 nm is presented. Two strongly stained islands of BCC can be clearly delineated in the image. Magnified confocal images of the BCC lobule, which is outlined in red in Fig. 8(a), acquired at 660 nm (strong absorption by MB) and 830 nm (negligible absorption by MB) are shown in Figs. 8(b) and 8(c), respectively. Detailed evaluation of confocal images taken at 660 and 830 nm demonstrates that one part of the suspicious area (marked with green arrow) appears dark in both images, whereas another part (marked with red arrow) is much darker in 660 nm, as compared to the 830-nm image. Therefore, the area that is clearly darker in the 630-nm image than in the 830-nm image contains a significant amount of the dye and can be presumed to be a tumor. However, the suspicious area that is dark at both wavelengths implies a structure with low scattering and comparatively low dye uptake. In skin, sebaceous glands appear as such lower-scattering structures. Comparison of the images to histology, presented in Fig. 8(d) confirms that these dark areas contain a tumor lobule and a sebaceous gland (red and green arrows, respectively).

In total, we have investigated 23 thick surgical excisions of nonmelanoma skin cancer, including 18 basal cell carcinoma (nodular and infiltrative) and 5 invasive squamous cell carcinoma samples. The lateral size of the nonmelanoma skin cancer specimens varied from 4 to 36 mm and the thickness from

3 to 18 mm, respectively. The lateral sizes of the tumors ranged from 0.5 to 15 mm. For 13 tumors with lateral sizes less than 8×6 mm, confocal mosaics were created and qualitatively compared to superficial macroimages and histopathology (representative images are shown in Figs. 4 and 5). In all cases, the locations of the tumors were correctly determined in the superficial macroimages and in the confocal images, acquired at 630 and 660 nm for the samples stained in TB and MB, respectively. The shape and size of the tumor lobules found in confocal and superficial macroimages correlated well with corresponding histopathology. For all samples, the interesting features such as tumor lobules, sebaceous glands, hair follicles, etc., were identified and compared to histopathology (see representative images presented in Figs. 6, 7, and 8). The comparison confirmed that tissue structures have similar appearance in the images and histopathology.

This study demonstrates that polarized light macroimaging and confocal mosaics are a useful combination for delineation of nonmelanoma skin cancer margins in both BCC and SCC. Polarized light macroimaging is better than CM for macroscopic assessment, as it gives a larger field of view (~2.9×2.7 cm) almost instantaneously (~100 msec), does not require scanning or contact with tissue, and is not susceptible to patient movement. Confocal images acquired at a wavelength within the absorption band of a tumor-specific dye allow delineation of single tumor lobules, with contrast and resolution comparable to those of conventional histopathology. Rapid acquisition of confocal images at several wavelengths helps to discriminate cancer lobules with high dye concentration from healthy tissues with comparatively low scattering. It is not difficult to localize small structures in the tissue using confocal microscopy after a high-contrast dye-enhanced macroimage has been acquired. Synergy between these two optical techniques implies that the combination could be successfully used for intraoperative assessment of nonmelanoma skin cancer margins. Similar appearance of different tissue structures in histological sections and our images simplifies the process of image understanding. It ensures that image interpretation can be performed by a pathologist without any assistance.

In conclusion, MSPLI enables rapid imaging of large surfaces, but does not provide information on cellular microstructure. CM allows imaging with resolution comparable to histology, but suffers from small field of view. The combination of MSPLI and CM offsets the specific limitations of each technique alone, and may in practice rival conventional histo-

pathology. By allowing the tumor to be delineated *in situ*, this approach may decrease the cost and time of cancer surgery.

Acknowledgments

We thank Milind Rajadhyaksha and Salvador Gonzalez for helpful discussions. Technical support of Lucid, Incorporated (Henrietta, New York) is gratefully acknowledged. This research is supported in part by National Institutes of Health (R01 EB002423-01).

References

1. M. Rajadhyaksha, R. R. Anderson, and R. H. Webb, "Video-rate confocal scanning laser microscope for imaging human tissues *in vivo*," *Appl. Opt.* **10**, 2105–2115 (1999).
2. G. Wagnieres, W. Star, and B. C. Wilson, "In vivo fluorescence spectroscopy and imaging for oncological applications," *Photochem. Photobiol.* **68**, 603–632 (1998).
3. S. A. Boppart, B. E. Bouma, C. Pitris, G. J. Tearney, J. F. Southern, M. E. Brezinski, and J. G. Fujimoto, "Intraoperative assessment of microsurgery with three-dimensional optical coherence tomography," *Radiology* **208**, 81–6 (1998).
4. K. C. New, W. M. Petroll, A. Boyde, et al., "In vivo imaging of human teeth and skin using real-time confocal microscopy," *Scanning* **13**, 369–372 (1991).
5. M. Rajadhyaksha, M. Grossman, D. Esterowitz, R. H. Webb, and R. R. Anderson, "In vivo confocal scanning laser microscopy of human skin: melanin provides strong contrast," *J. Invest. Dermatol.* **104**, 946–952 (1995).
6. M. Rajadhyaksha, G. Menaker, P. J. Dwyer, T. J. Flotte, and S. Gonzalez, "Confocal examination of nonmelanoma cancers in skin excisions to potentially guide Mohs micrographic surgery without frozen histopathology," *J. Invest. Dermatol.* **117**, 1137–1143 (2001).
7. A. N. Yaroslavsky, V. Neel, and R. R. Anderson, "Demarcation of nonmelanoma skin cancer margins using multi-spectral polarized-light imaging," *J. Invest. Dermatol.* **121**, 259–266 (2003).
8. S. L. Jacques, J. R. Roman, and K. Lee, "Imaging superficial tissues with polarized light," *Lasers Surg. Med.* **26**, 119–129 (2000).
9. V. Backman, M. Wallace, L. T. Perelman, et al., "Detection of pre-invasive cancer cells. Early-warning changes in precancerous epithelial cells can now be spotted *in situ*," *Nature (London)* **406**(6791), 35–36 (2000).
10. A. R. Oseroff, D. Ohuoha, G. Ara, D. McAuliffe, J. Foley, and L. Cincotta, "Intramitochondrial dyes allow selective *in vitro* photolysis of carcinoma cells," *Proc. Natl. Acad. Sci. U.S.A.* **83**, 9729–9733 (1986).
11. R. A. Drezek, T. Collier, C. K. Brookner, A. Malpica, R. Lotan, and R. R. Richards-Kortum, "Laser scanning confocal microscopy of cervical tissue before and after application of acetic acid," *Am. J. Obstet. Gynecol.* **182**, 1135–1139 (2000).
12. F. E. Mohs, "Chemosurgery—a microscopically controlled method of cancer excision," *Arch. Surg. (Chicago)* **42**, 279–295 (1941).
13. *Mohs Surgery: Fundamentals and Techniques*, K. G. Gross, H. K. Steinman, and R. P. Rapini, Eds., Mosby, Inc. (1999).